2018 European Control Conference (ECC)
June 12-15, 2018. Limassol, Cyprus

Control design oriented modeling of an on-ground aircraft

Ejagen Sadien[⋆,†,◇], Clément Roos[†], Abderazik Birouche[◇], Christophe Grimault[⋆], Louis Emmanuel Romana[⋆], Josep Boada-Bauxell[⋆] and Michel Basset[◇]

Abstract— **The aim of this paper is to present a simple yet accurate design-oriented on-ground aircraft model, during the roll-out and take-off phases between 40 and 100 knots, with 3 degrees of freedom (DOF). The proposed model takes into account the effects of aerodynamics, thrust and tire-ground interaction, both laterally and longitudinally, under several runway states. The on-ground dynamics of the aircraft can be controlled by engines thrust, rudder deflection, nose wheel steering and (differential) braking, whose physical limitations are considered. It is validated against an in-house high-fidelity Airbus simulator. A complete set of numerical values representative of a commercial aircraft is included, as well as design objectives, so as to provide the control community with a challenging benchmark.**

I. INTRODUCTION

Many airborne phases of commercial flights have been automated with the development of fly-by-wire solutions [1]. However, after touchdown, the motion of the aircraft is usually controlled manually by the pilot using: throttle levers, rudder pedals, handwheels and brake pedals. This is especially demanding in adverse conditions such as contaminated runways and severe crosswinds. Following a study carried out by the International Civil Aviation Organization (ICAO) during the Global Runway Safety Symposium 2011, the count of runway excursions has not decreased over the last 20 years [2]. Factors leading to runway excursions analyzed in [3] are mainly due to wet/contaminated runways, crosswinds and nose wheel steering problems. Nevertheless, automation is possible under constraining ground infrastructure and operational requirements.

The complexity of aircraft ground dynamics lies in the coupling of aerodynamic effects and tire-road interactions, the latter being highly nonlinear and depending on various parameters such as runway characteristics and conditions, tire characteristics, anti-skid braking system, longitudinal speed of the aircraft, etc. This is illustrated in [4] and references therein, where the on-ground lateral dynamics of a mid-size commercial aircraft are studied comprehensively. In these papers, a bifurcation analysis is carried out to investigate the aircraft cornering behavior in relation to longitudinal speed, nose wheel steering angle and rate, tire-ground friction and position of the center of gravity. Apart from tire-road interaction, nonlinearities are also introduced by actuator limitations and thus, form a core part of the aircraft model. But such high-complexity models with at least 6 DOF are more convenient for analysis and validation than for control.

On the other hand, some simplified design-oriented models have been developed, which usually focus on the lateral behavior of the aircraft [5], [6], [7]. Some papers consider both the longitudinal and the lateral behaviors but they do not discuss the coupling effects or do not provide a complete modeling of the tire-road interactions [8], [9], [10]. The operational domain is sometimes limited to low speed [5] and if higher speed is considered, only the rudder is usually taken into account in addition to the nose-wheel steering system [6], [8], [7], except [10] which introduces an engine model, and [9] which considers all available actuators including the braking system.

Several design strategies have been proposed to control the aircraft at low speed using the nose-wheel steering system, see *e.g.* [11]. Moreover, a lot of progress has been made in the longitudinal energy management and control [12], [13], namely the Brake To Brake function developed by Airbus [14]. But one of the most challenging on-ground control problems occurs at intermediate speed between 40 and 100 knots. The main objective is runway axis hold, *i.e.* ensuring that the lateral deviation Y_G remains acceptable despite wind, different runway states and comfort constraints, while minimizing brakes wear. But none of the aforementioned simplified models can be used to address this open issue. Indeed, achieving good performance during this worst-case scenario makes it necessary to combine all available actuators, which gives rise to a control allocation problem, and to take into account the runway state and the most important non-linearities of the system.

In this context, the main contribution of this paper is to bridge the gap between high-complexity representations and over-simplified ones, in order to address advanced control problems such as the one described above. The proposed model takes into account all existing actuators (nose-wheel steering system, rudder, engines and brakes) including their dynamics and limitations. It considers both longitudinal and lateral contact forces in a novel way, including rolling resistance and slip forces. Simple dependencies to the vertical load and the runway state are also taken into account. An accurate yet tractable 3 DOF model is finally obtained, which can be easily trimmed and linearized for design purposes.

The paper is organized as follows. The proposed control design oriented model is thoroughly described in Section II, and then compared to a high-fidelity simulator in Section III.

[⋆]Airbus Operations S.A.S., Toulouse, France. E-mail: ejagen.sadien@airbus.com, christophe.grimault@airbus.com, louis-emmanuel.romana@airbus.com, josep.boada-bauxell@airbus.com.

[†]ONERA, The French Aerospace Lab, Toulouse, France. E-mail: clement.roos@onera.fr

[◇]IRIMAS, Université de Haute-Alsace, Mulhouse, France. E-mail: abderazik.birouche@uha.fr, michel.basset@uha.fr

II. AIRCRAFT MODELING

A. General Equations and Simplifying Assumptions

Following a classical approach, the motion of an aircraft, of mass m and inertia matrix I_p, defined at its center of gravity *G*, is given by:

$$\begin{bmatrix}\dot{\vec{V}}\\ \dot{\vec{\Omega}}\end{bmatrix} = \begin{bmatrix}\vec{F}/m - \vec{\Omega}\wedge\vec{V}\\ {I_p}^{-1}(\vec{M} - \vec{\Omega}\wedge I_p\vec{\Omega})\end{bmatrix} \quad (1)$$

where $\vec{V} = [V_x\ V_y\ V_z]^T$, $\vec{\Omega} = [p\ q\ r]^T$ denote the linear and angular velocity vectors, and $\vec{F} = [F_x\ F_y\ F_z]^T$, $\vec{M} = [M_p\ M_q\ M_r]^T$ are the total external forces and moments acting on the aircraft at *G*. Unless otherwise specified, all vectors are expressed in the direct orthonormal body reference system $\mathcal{R}_b$ described in Fig. 1.

The proposed model is valid for an aircraft on the runway during both take-off and landing, excluding maneuvers on the taxiway. The following assumptions are made in order to simplify the general nonlinear equations, yielding a model of tractable complexity adapted for control design:

(A1) Tricycle hypothesis.
(A2) Linearized expressions for the modeling of aerodynamic effects, with deployed ground spoilers, setting a speed upper bound of 100 knots.
(A3) Rigid aircraft and shock absorbers, *i.e.* planar motion ($p = q = 0;\ V_z = 0$), yielding same load on left and right main landing gears.
(A4) Symmetrical engines thrust T_{eng} (forward thrust, no reverse) aligned with the fuselage reference axis $\vec{x_b}$.
(A5) Small angles approximation, including the nose wheel steering angle θ_{NW}, implying a maximum crosswind of 5 knots in the $\vec{x_b}\vec{y_b}$ plane and a speed lower bound of 40 knots.
(A6) Velocity of main landing gears wheels center equal to that of *G*.

The small angles approximation and the limited horizontal crosswind assumed in *(A5)*, as well as the stationary behavior of the ground spoilers, allow to consider linearized equations for the aerodynamic effects, which justifies *(A2)*. But the assumption on the ground spoilers sets an upper bound on the speed domain. Then, tire sideslips mechanically get larger as speed decreases, and the saturation-based tire model developed in this paper becomes less accurate, especially below 40 knots. Moreover, maneuvers above 40 knots exclusively consist of keeping a straight trajectory on the runway, which is compatible with the small angles approximation of *(A5)*. This is not true below this limit, where the aircraft evolves on the taxiways. Finally, the largest error in the considered operating domain between the velocity of the main landing gears wheels center and that of G is obtained at low speed ($V_x = 40$ knots). Noting that the yaw rate r is no larger than 10 deg/s in practice, rDx_{MG} is negligible compared to V_y and an error of only 2% is obtained, which validates assumption *(A6)*. The other assumptions are standard and do not require any additional justification.

Remark 1: Models making use of saturation-based tire models suffer from the same speed lower bound limitation, see *e.g.* [8] and the *DESANA* longitudinal model in [15].

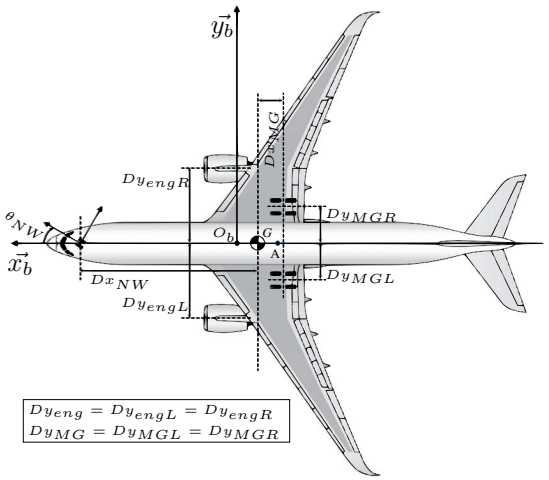

Fig. 1: Body reference system $\mathcal{R}_b$

Thanks to assumptions *(A1,A2,A3)*, equation (1) is reduced to a 3 DOF body motion:

$$\begin{aligned}\dot{V}_x &= F_x/m + rV_y\\ \dot{V}_y &= F_y/m - rV_x\\ \dot{r} &= M_r/I_{zz}\end{aligned} \quad (2)$$

where I_{zz} refers to the inertia around the $\vec{z_b}$ axis. The following kinematic equation then gives the aircraft heading ψ:

$$\dot{\psi} = r \quad (3)$$

The forces $\vec{F}$ and moments $\vec{M}$ acting on an on-ground aircraft are engines thrust, aerodynamic effects, weight and ground reaction forces, all expressed in $\mathcal{R}_b$. The longitudinal and lateral forces and yawing moment are denoted F_{xi}, F_{yi} and M_{ri} respectively, where i indicates engines thrust (eng), aerodynamic effects (a) or ground forces (g). The reference origin O_b is chosen to be the start position of the mean aerodynamic chord c. Thus, the weight and the aerodynamic effects can be considered to act at points located along $\vec{x_b}$ at G and A respectively, whose x-coordinates are $X_G = -c_G \cdot c$ and $X_A = -c_A \cdot c$, c_G and c_A being positive dimensionless coefficients.

The motion is planar according to assumption *(A3)*, so the weight does not intervene in the forces and the moment of interest, except in the normal reaction on the wheels. Then according *(A4)*, the thrust impacts only the longitudinal motion as $F_{xeng} = T_{eng}$. Considering the presence of wind disturbance $\vec{W} = [W_x\ W_y\ 0]^T$ in the $\vec{x_b}\vec{y_b}$ plane, the aerodynamic velocity $\vec{V_a}$ is defined hereafter in $\mathcal{R}_b$:

$$\vec{V_a} = [V_{ax}\ V_{ay}\ V_{az}]^T = \vec{V} - \vec{W} \quad (4)$$

Under assumptions *(A2,A3,A5)* and for simplicity reasons, the aerodynamic effects at *G* are linearized in $\mathcal{R}_b$ [16]:

$$\begin{aligned}F_{xa} &= q_d S C x_0\\ F_{ya} &= q_d S\left(Cy_\beta\beta + Cy_r\frac{rc}{V_a} + Cy_{\delta r}\delta r\right)\\ M_{ra} &= q_d Sc\left(Cn_\beta\beta + Cn_r\frac{rc}{V_a} + Cn_{\delta r}\delta r\right)\\ F_{za} &= q_d S C z_0\end{aligned} \quad (5)$$

where V_a is the Euclidean norm of $\vec{V_a}$, and $q_d = \frac{1}{2}\rho {V_a}^2$ and S are the dynamic pressure and the reference surface respectively. In addition, Cx_0, Cy_j, Cn_j and Cz_0 refer to the drag, lateral, yaw and lift stability derivatives whereby j denotes the effect due to aerodynamic sideslip angle (β), yaw rate (r) or rudder deflection (δr). Note that $V_z = W_z = V_{az} = 0$ according to assumptions *(A3,A5)*, so the angle of attack is zero, which explains why the drag and lift coefficients are constant.

Remark 2: Under assumption *(A5)*, the sideslip angle is approximated by $\beta = \arcsin\left(V_{ay}/V_a\right) \approx V_{ay}/V_a$.

Remark 3: The lift F_{za} affects the normal reaction on each landing gear and in turn the contact forces (see Section II-B).

B. Contact Force Model

A tire in motion is subject to normal reaction F_{z_k}, rolling resistance F_{r_k}, braking torque T_{brk_k} and slip forces F_{sx_k} and F_{sy_k}, the latter arising from the presence of either longitudinal or lateral slip between the contact patch and the ground. These forces are shown in Fig. 2b for a main landing gear wheel. They act along the $\vec{x_k}$ and $\vec{y_k}$ axes of the tire, where k refers to the nose wheel (NW) or the left (resp. right) main landing gear wheel (MGL (resp. MGR)), as defined in Fig. 2a (see [17] for tire modeling).

Normal Reaction: The nose wheel is a free rolling wheel (*i.e.* neither driven nor braked) and therefore is subject to rolling resistance F_{r_k} and lateral slip force F_{sy_k}. The main landing gears wheels are potentially braked and therefore experience not only the aforesaid forces but also longitudinal slip forces F_{sx_k}. These forces depend primarily on the normal reaction F_{zk} at each landing gear. Thanks to assumption *(A3)*, moment balances around the $\vec{y_b}$ axis at the nose and main landing gears wheels yield:

$$\begin{aligned} F_{z_{NW}} &= \frac{mgD_{xMG} - F_{za}\left(D_{xMG} - c\left(c_A - c_G\right)\right)}{D_{xNW} + D_{xMG}} \\ F_{z_{MGR/L}} &= \frac{mgD_{xNW} - F_{za}\left(D_{xNW} + c\left(c_A - c_G\right)\right)}{2\left(D_{xNW} + D_{xMG}\right)} \end{aligned} \tag{6}$$

where D_{xNW} and D_{xMG} are positive distances shown in Fig. 1 and g is the standard gravity.

Remark 4: The normal reaction forces are defined positive along the $-\vec{z_b}$ axis.

Rolling Resistance: Rolling resistance arises due to the hysteresis of rubber during deformation of the tire and is considered as proportional to F_{z_k}. Other models exist whereby the rolling friction coefficient μ_r is function of powers of the longitudinal speed [18], temperature and pressure, but they are not considered here for the sake of simplicity. The rolling resistance F_{rk} acts backwards along the $-\vec{x_k}$ axis as shown in Fig. 2b and is given by:

$$F_{r_k} = \mu_r F_{z_k} \tag{7}$$

where $\mu_r = \bar{\mu}\mu_{rMAX}$ depends on the characteristics of the surface in contact with the wheels. The relative friction

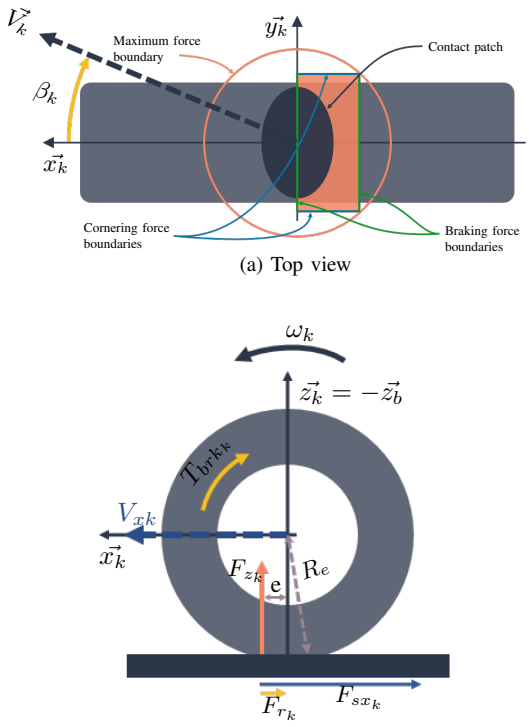

(a) Top view

(b) Side view

Fig. 2: Wheel reference system and forces/moments

coefficient $\bar{\mu}$ depends on the runway state, and is typically equal to 1 for dry, 0.74 for wet and 0.29 for snowy runway. μ_{rMAX} denotes the maximum rolling friction coefficient considered for a dry runway.

Lateral Sideslip Angles: The lateral slip forces F_{sy_k} do not only depend on normal reaction but are also function of the sideslip angles β_k. Under assumptions *(A1,A3,A5,A6)*, β_k can be computed as [18]:

$$\begin{aligned} \beta_{NW} &= \frac{V_y + rDx_{NW}}{V_x} - \theta_{NW} \\ \beta_{MGR} &= \beta_{MGL} \underbrace{=}_{(A6)} \beta_G = \frac{V_y}{V_x} \end{aligned} \tag{8}$$

Slip Force Model: A simplified model is proposed in [8], where the slip force is represented by a saturated linear function in the case of pure lateral slip:

$$F_{sy_k} = -N_{t_k}\ \mathrm{sat}_{\left[\bar{\mu}F_{syMAX_k}\right]}\left(G_{y_k}\beta_k\right) \tag{9}$$

The saturation level $\bar{\mu}F_{syMAX_k}$ depends on the runway state and the maximum lateral force F_{syMAX_k} for a dry runway. N_{t_k} denotes the number of tires in the considered landing gear and the cornering gain $G_{y_k} = \left.\frac{\partial F_{sy_k}}{\partial \beta_k}\right|_{\beta_k=0}$ is computed for a mean value of the normal reaction. No explicit dependency of G_{y_k} on F_{z_k} is considered in [8], but an uncertainty is introduced on G_{y_k}, whose bounds are determined thanks to extensive simulations. This is illustrated in Fig. 3, where the nominal model (9) is shown by the green dashed line, while the bounds on the uncertain cornering

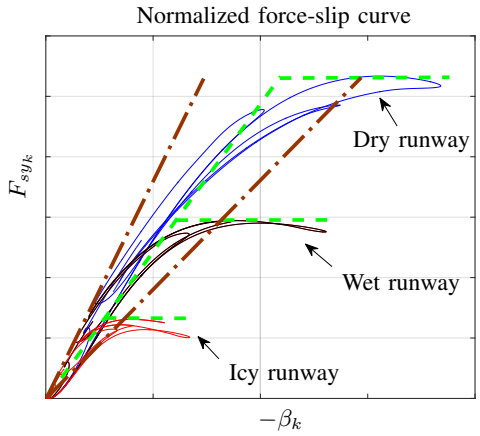

Fig. 3: Lateral slip model proposed in [8]

gain are displayed by the brown dot-dashed lines. The saturation operator is defined such that $\text{sat}_{[F]}(x) = x$ if $|x| < F$ and $\text{sat}_{[F]}(x) = F\ \text{sign}(x)$ otherwise. Based on [8], an improved model is proposed in this paper, which accounts for combined slip, runway state and normal load variation. The combined lateral and longitudinal slip forces $F_{s_k} = \sqrt{F_{sx_k}^2 + F_{sy_k}^2}$ generated considering an isotropic tire under non-zero sideslip and longitudinal slip cannot exceed μF_{z_k} [19], where $\mu = \bar{\mu}\mu_{MAX}$ denotes the tire-road friction coefficient and μ_{MAX} its maximum value corresponding to a dry runway. The maximum force boundary is illustrated by the orange circle in Fig. 2a. The idea to avoid this coupling between F_{sx_k} and F_{sy_k} is to assume that the sideslip angles β_k remain small during the roll-out phase, typically less than 5 degrees in practice. Furthermore, the anti-skid system prevents the longitudinal slip ratio of becoming too large. In this context, it can be reasonably assumed that the resultant of the slip forces lies inside the orange area instead of the orange circle in Fig. 2a, where the longitudinal and lateral maximum forces are represented in green and blue respectively. The following model is then assumed:

$$F_{sx_k} = N_{t_k}\ \text{sat}_{\left[\bar{\mu}\lambda_{sx_k}\frac{F_{z_k}}{N_{t_k}}\right]}\left(K_{x_k}T_{brk_k}\right) \tag{10a}$$

$$F_{sy_k} = -N_{t_k}\ \text{sat}_{\left[\bar{\mu}\lambda_{sy_k}\frac{F_{z_k}}{N_{t_k}}\right]}\left(K_{y_k}\beta_k\frac{F_{z_k}}{N_{t_k}}\right) \tag{10b}$$

where K_{x_k}, K_{y_k} correspond to the inverse of the effective rolling radius R_e and the reduced lateral cornering gain (defined positive per unit normal reaction) respectively, and λ_{sx_k}, λ_{sy_k} denote the longitudinal and lateral friction fractions, defined for a dry runway and satisfying ${\lambda_{sx_k}}^2 + {\lambda_{sy_k}}^2 = {\mu_{MAX}}^2$. The saturation levels depend on various parameters, but for simplicity, they are considered here to be proportional to the normal reaction and the relative runway friction coefficient. K_{y_k} is considered independent of speed in the operational domain but depending on the runway state according to [20]:

$$K_{y_k} = \frac{K_{yMAX_k}}{\frac{2}{3} + \frac{1}{3\bar{\mu}}} \tag{11}$$

where K_{yMAX_k} denotes the reduced lateral cornering gain defined for a dry runway.

Remark 5: Under a fixed braking torque, the average longitudinal slip force F_{sx_k} remains constant when longitudinal velocity is not null and the wheel keeps rolling [18], which verifies (10a) in the considered operational domain. Moreover, the inner control loop of the braking system linearizes the torque-force transfer to compensate brake gain variations and the ABS prevents the lock of the wheel.

Remark 6: If aircraft tires are subject to large load variations, the explicit consideration of the normal reaction in (10) is coherent considering the use case with small sideslip angles [17].

Summary of Contact Forces and Moments: Under assumption *(A5)*, $\sin\theta_{NW}$ and $\cos\theta_{NW}$ can be replaced with θ_{NW} and 1 respectively. The total contact forces and moments at G in $\mathcal{R}_b$ are thus:

$$\begin{aligned} F_{xg} &= -F_{r_{NW}} - F_{r_{MGR}} - F_{r_{MGL}} \\ &\quad -F_{sy_{NW}}\theta_{NW} - F_{sx_{MGR}} - F_{sx_{MGL}} \\ F_{yg} &= -F_{r_{NW}}\theta_{NW} + F_{sy_{NW}} \\ &\quad +F_{sy_{MGR}} + F_{sy_{MGL}} \\ M_{rg} &= \left(F_{sy_{NW}} - F_{r_{NW}}\theta_{NW}\right) D_{xNW} \\ &\quad -\left(F_{sy_{MGR}} + F_{sy_{MGL}}\right) D_{xMG} \\ &\quad +\left(F_{sx_{MGR}} + F_{r_{MGR}}\right) D_{yMG} \\ &\quad -\left(F_{sx_{MGL}} + F_{r_{MGL}}\right) D_{yMG} \end{aligned} \tag{12}$$

C. Actuators and Engines Models

In the operational domain defined in Section II-A, the aircraft is controlled by the engines, the brakes located on the left and right main landing gears, the nose wheel steering system and the rudder. The engines are considered as quasi-static and approximated by a first order dynamic model of unit gain and time constant τ_{eng}, with position limitation $L_{peng} = [T_{engIDLE},\ T_{engMAX}]$. The thrust limitation is due to mechanical stops of the throttle, further limited by the operating domain between the Idle Forward and maximum thrust positions as described below:

$$\tau_{eng}\dot{T}_{eng} + T_{eng} = T_{eng_c} \text{ with } T_{eng} \in L_{peng} \tag{13}$$

where T_{eng_c} is the commanded thrust. The right (resp. left) braking system is approximated by a first order dynamic model of nominal gain G_{brk} and time constant τ_{brk}, with position L_{pbrk} and rate L_{rbrk} limitations. However, braking starts only if the pressure P_{brk_k} is above a threshold P_0, so as to overcome the restoring force of springs located between the brake discs and the brake pistons:

$$\tau_{brk}\dot{P}_{brk_k} + P_{brk_k} = P_{brk_{k_c}} \text{ with } \begin{cases} 0 \le P_{brk_k} \le L_{pbrk} \\ |\dot{P}_{brk_k}| \le L_{rbrk} \end{cases} \tag{14}$$

$$T_{brk_k} = \max\left(0, G_{brk}\left(P_{brk_k} - P_0\right)\right)$$

The nose wheel steering (resp. the rudder) actuation system is approximated by a first order dynamic model of time

constant τ_{NW} (resp. $\tau_{\delta r}$) with position L_{pNW} and rate L_{rNW} limitations (resp. $L_{p\delta r}$ and $L_{r\delta r}$):

$$\tau_{NW}\dot{\theta}_{NW} + \theta_{NW} = \theta_{NW_c} \text{ with } \begin{cases} |\theta_{NW}| \leq L_{pNW} \\ |\dot{\theta}_{NW}| \leq L_{rNW} \end{cases} \quad (15)$$

$$\tau_{\delta r}\dot{\delta r} + \delta r = \delta r_c \text{ with } \begin{cases} |\delta r| \leq L_{p\delta r} \\ |\dot{\delta r}| \leq L_{r\delta r} \end{cases}$$

D. Model Summary

The model structure is illustrated in Fig. 4a. The *Act* block contains the engine model, as well as the nose wheel steering, braking and rudder actuator models. The aerodynamic effects and the contact forces are computed in the *F&M* block, whose structure is further decomposed as shown in Fig. 4b. Equations of motion (2) are implemented in the *EoM* block. To sum up, the model is composed of:

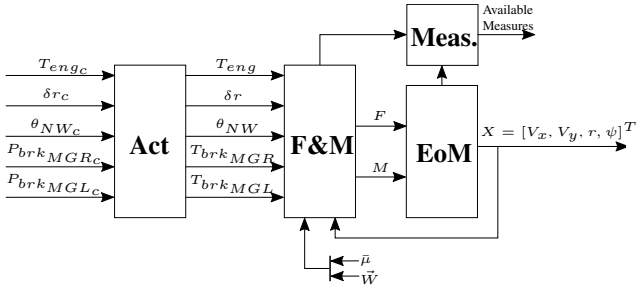

(a) Global architecture

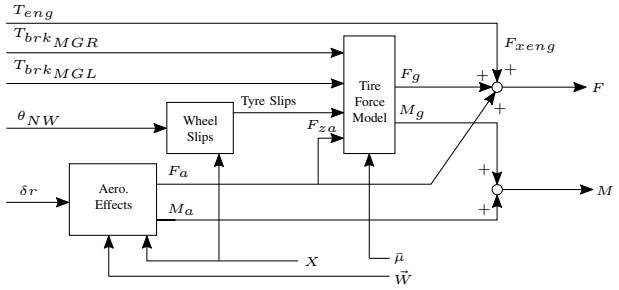

(b) Forces and moments (F&M) architecture

Fig. 4: Proposed model

- 5 control inputs: $\delta r_c, \theta_{NW_c}, P_{brk_{MGR_c}}, P_{brk_{MGL_c}}, T_{eng_c}$,
- 2 wind disturbances: W_x, W_y,
- 9 states : V_x, V_y, r, ψ and 5 actuator states,
- 7 measured outputs: $V_x, V_y, N_x, N_y, r, \dot{r}, \theta_{NW}$, where $N_x = \frac{\dot{V}_x}{g}$ and $N_y = \frac{\dot{V}_y}{g}$ are the longitudinal and lateral load factors.

Each sensor is represented by a first order filter of unit gain and time constant τ_{sensor}, and a delay τ_{delay}. A complete set of numerical nominal values representative of a commercial aircraft is provided in TABLE I. These values may not be known with accuracy, therefore uncertainties on the stability derivatives, the cornering stiffness, and also the runway state (impacted by badly known external conditions), can be considered.

III. MODEL VALIDATION

The proposed model is compared to a high-fidelity Airbus simulator in order to assess the effectiveness of the contact forces and actuators models. The simulator has been developed for control laws validation purposes [21] and is valid in the whole aircraft operating domain, including ground phases. Three maneuvers during the roll-out phase, with the engines at idle, are considered:

Parameter	Unit	Typical value
m	kg	60×10^3
I_{zz}	kg.m^2	3.70×10^6
S	m^2	122
c	m	4.2
c_G / c_A	-	0.30 / 0.42
$DxNW$ / $DxMG$ / $DyMG$	m	11.45 / 1.19 / 3.80
Cx_0 / Cz_0	-	-0.090 / 0.905
Cy_β / Cn_β	-	-1.36 / 2.50
Cy_r / Cn_r	-	3.69 / -16.29
$Cy_{\delta r}$ / $Cn_{\delta r}$	-	0.34 / -2.01
μ_{rMAX} / μ_{MAX}	-	0.015 / 0.68
$K_{yMAX_{NW}}$ / $K_{yMAX_{MG}}$	/rad	408 / 400
R_e	m	0.50
$\lambda_{sy_{NW}}$ / $\lambda_{sy_{MG}}$ / $\lambda_{sx_{MG}}$	-	0.68 / 0.45 / 0.51
$N_{t_{NW}} = N_{t_{MGR}} = N_{t_{MGL}}$	-	2
τ_{sensor} / τ_{delay}	s	1×10^{-3} / 5×10^{-2}
τ_{eng} / τ_{brk} / τ_{NW} / $\tau_{\delta r}$	s	2 / 10^{-3} / 0.1 / 0.2
$T_{engIDLE}$ / T_{engMAX}	N	10×10^3 / 300×10^3
L_{pbrk} / P_0	Pa	175×10^5 / 15×10^5
L_{rbrk}	Pa/s	20×10^5
G_{brk}	Nm/Pa	4×10^{-3}
L_{pNW} / $L_{p\delta r}$	deg	74 / 30
L_{rNW} / $L_{r\delta r}$	deg/s	20 / 30

TABLE I: Benchmark values

- *Maneuver 1*: $\pm$ 4 deg trapezoidal-doublet of the hand-wheel on a snowy runway at low speed.
- *Maneuver 2*: right then left 3 deg trapezoidal brake pedal deflection on a wet runway at medium speed.
- *Maneuver 3*: $\pm$ 2 deg trapezoidal-doublet of the rudder pedal deflection on a dry runway at high speed.

The time responses of V_y, r, β_{NW} and Y_G for maneuvers 1 to 2 are shown in Fig. 5 and 6 to assess the lateral characteristics of the aircraft, where Y_G denotes the lateral deviation of the center of gravity with respect to the runway centerline. The simulator responses are given by blue solid lines and those of the proposed model by black dashed lines. The main objective is runway axis hold, therefore the longitudinal characteristics are not shown. The vertical axes are normalized since they contain Airbus proprietary data.

Remark 7: Maneuver 3 yields similar results as maneuvers 1 and 2 and is not reported by lack of space.

In all cases, the lateral behavior of the proposed model is close to that of the simulator. As depicted in Fig. 5 and 6, the error is mainly on the peak values. This can be due to assumption *(A3)*, *i.e.* no vertical load transfer, and to the transient wheel dynamics which is not considered in this study. Hence, the proposed model is well-suited for the development of ground control laws, so as to ensure runway axis hold and longitudinal control between 40 and 100 knots using symmetric thrust, rudder deflection, nose-wheel steering and differential braking.

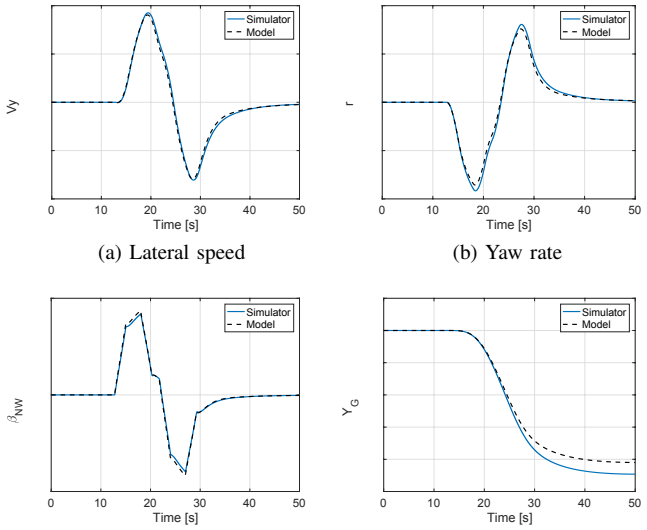

(a) Lateral speed (b) Yaw rate

(c) Nose-wheel sideslip angle (d) Lateral excursion

Fig. 5: Maneuver 1: handwheel order

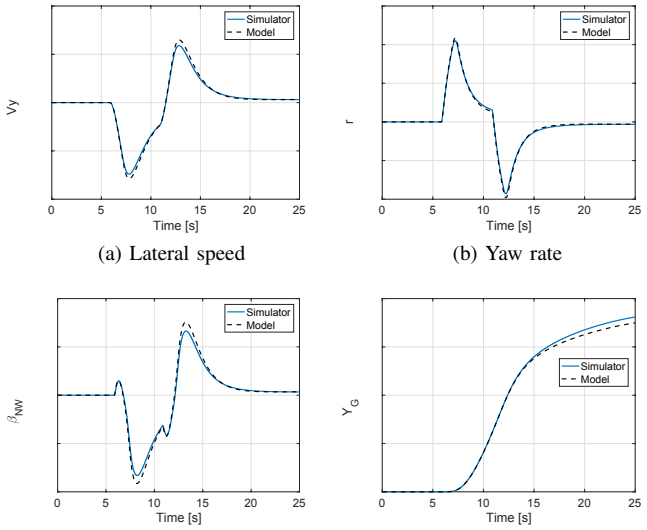

(a) Lateral speed (b) Yaw rate

(c) Nose-wheel sideslip angle (d) Lateral excursion

Fig. 6: Maneuver 2: differential braking order

IV. CONCLUSION

In this paper, a new simple yet tractable design-oriented model of an on-ground aircraft is developed. Despite its simplicity, it approximates quite well a high-fidelity in-house Airbus simulator in the operational range between 40 and 100 knots, where the main objective is runway axis hold. It is used in [22], where a first attempt is made to solve the resulting control allocation problem. Future works shall be dedicated to the development of a 6 DOF model taking into consideration phenomena such as dynamic load transfers, castering during steering, gear walk during braking and wheel dynamics. Thus, the operating domain will be extended to include severe crosswinds.

ACKNOWLEDGMENT

This research is supported by Airbus Operations S.A.S., the National Association of Research and Technology (ANRT) and the French Ministry of Higher Education, Research and Innovation under the *CIFRE* contract number 2016/1058.

REFERENCES

[1] P. Traverse, I. Lacaze, and J. Souyris, "Airbus fly-by-wire: A total approach to dependability," in *Proceedings of the 18th IFIP World Computer Congress*, Toulouse, France, August 2004, pp. 191 – 212.

[2] Eurocontrol, "European action plan for the prevention of runway excursions edition 1.0," Eurocontrol, Tech. Rep., January 2013.

[3] G. W. H. van Es, "A study of runway excursions from a european perspective," Eurocontrol, Tech. Rep. NLR-CR-2010-259, May 2010.

[4] J. Rankin, B. Krauskopf, M. Lowenberg, and E. Coetzee, "Nonlinear analysis of lateral loading during taxiway turns," *Journal of Guidance, Control and Dynamics*, vol. 33, no. 6, pp. 1708 – 1717, 2010.

[5] D. Lemay, Y. Chamaillard, M. Basset, and J. P. Garcia, "Gain-scheduled yaw control for aircraft ground taxiing," in *Proceedings of the 18th IFAC World Congress*, Milan, Italy, August 2011, pp. 12 970 – 12 975.

[6] C. Bihua, J. Zongxia, and S. S. Ge, "Aircraft-on-ground path following control by dynamical adaptive backstepping," *Chinese Journal of Aeronautics*, vol. 26, no. 3, pp. 668 – 675, 2013.

[7] G. Looye, "Chapter 8: Rapid prototyping using inversion-based control and object-oriented modelling," in *Nonlinear Analysis and Synthesis Techniques for Aircraft Control*. Lecture Notes in Control and Information Sciences, vol. 365, Springer, 2007, pp. 147 – 173.

[8] J.-M. Biannic, A. Marcos, M. Jeanneau, and C. Roos, "Nonlinear simplified LFT modelling of an aircraft on ground," in *Proceedings of the IEEE International Conference on Control Applications*, Munich, Germany, October 2006, pp. 2213 – 2218.

[9] M. C. Turbuk and P. Paglione, "Aircraft ground dynamics modeling," in *Proceedings of the VI National Congress of Mechanical Engineering*, Campina Grande, Paraiba, Brazil, August 2010.

[10] H. Georgieva and V. Serbezov, "Mathematical model of aircraft ground dynamics," in *Proceedings of the 2017 International Conference on Military Technologies (ICMT)*, Brno, Czech Republic, June 2017, pp. 514 – 519.

[11] C. Roos, J.-M. Biannic, S. Tarbouriech, C. Prieur, and M. Jeanneau, "On-ground aircraft control design using a parameter-varying anti-windup approach," *Aerospace Science and Technology*, vol. 14, no. 7, pp. 459 – 471, 2010.

[12] F. Villaumé, "Contribution à la commande des systèmes complexes : Application à l'automatisation du pilotage au sol des avions de transport," Ph.D. dissertation, Université Toulouse III - Paul Sabatier, Toulouse, France, February 2002.

[13] J. Duprez, F. Mora-Camino, and F. Villaumé, "Control of the aircraft-on-ground lateral motion during low speed roll and manoeuvers," in *Proceedings of the 2004 IEEE Aerospace Conference Proceedings*, March 2004, pp. 2656 – 2666.

[14] F. Villaumé and T. Lagaillarde, "Fast: Runway overrun prevention system (ROPS)," Airbus, Tech. Rep. 55, January 2015, http://www.aircraft.airbus.com/support-services/publications/.

[15] A. Marcos, J.-M. Biannic, M. Jeanneau, D. G. Bates, and I. Postlethwaite, "Aircraft modelling for nonlinear and robust control design and analysis," in *Proceedings of the 5th IFAC Symposium on Robust Control Design*, Toulouse, France, July 2006, pp. 679 – 684.

[16] R. F. Stengel, *Flight Dynamics*. Princeton University Press, 2015.

[17] R. Kiébré, "Contribution to the modelling of aircraft tyre-road interaction," Ph.D. dissertation, Université de Haute-Alsace, Mulhouse, France, December 2010.

[18] H. Pacejka, *Tire and Vehicle Dynamics*, 3rd ed. Elsevier, 2016.

[19] R. Brach and M. Brach, "The tire-force ellipse (friction ellipse) and tire characteristics," SAE International, Tech. Rep. 2011-01-0094, December 2011.

[20] D. J. Mitchell, "Frictional and retarding forces on aircraft tyres part IV: Estimation of effects of yaw," ESDU, Tech. Rep. 86016a, April 2006.

[21] P. Goupil, J. Boada-Bauxell, A. Marcos, E. Cortet, M. Kerr, and H. Costa, "Airbus efforts towards advanced real-time fault diagnosis and fault tolerant control," in *Proceedings of the 19th IFAC World Congress*, Cape Town, South Africa, August 2014, pp. 3471 – 3476.

[22] M. Cassaro, C. Roos, and J.-M. Biannic, "Robust dynamic allocation for aircraft roll-out phase directional control," in *Proceedings of the 2018 European Control Conference*, Limassol, Cyprus, June 2018.